Numerical Investigation of Single Large Bubble Injection in Turbulent Channel Flow

◯   Sang-Won Kim, Hokkaido Univ., Hokkaido, Japan 060-8626, swkim5834@eis.hokudai.ac.jp

Nobuyuki Oshima, Hokkaido Univ., Hokkaido, Japan 060-8626, oshima@eng.hokudai.ac.jp

Yuichi Murai, Hokkaido Univ., Hokkaido, Japan 060-8626, murai@eng.hokudai.ac.jp

Hyun Jin, Park, Hokkaido Univ., Hokkaido, Japan 060-8626, park@eng.hokudai.ac.jp

Injection of bubbles into a turbulent boundary layer has multiple impacts, and frictional drag reduction is a phenomenon from their combined effect. Large bubble, around $We \geq 100$, show large area of drag reduction than small and micro bubble. However, it is hard to maintain their shape (when critical we is around 10 cause unstable and fragment into multiple small bubbles) and prone to deform in turbulent flow. Thus, the research objectives are checking the capability of simulation on large bubble and establishing numerical procedure how to inject the large bubble on turbulent channel flow without breakup. In addition, understanding its characteristic such as. the surrounding flow phenomena was performed.

1. Introduction

Recently, as growing concern about global warming, the international maritime organization (IMO) regulated the requirement about ship's greenhouse gas (GHG) emission. To reduce it, the air lubrication system is one of the solutions and shows good performance. Currently, most of the air lubrication systems are based on BDR which apply small, less than 0.1mm, and micro-bubble, but they have some drawback like difficulty to produce on a full-scale ship and less effective at low speeds due to buoyancy.

On the other hand, large bubble has great capability to reduce drag in large area as Fig. 1. These large bubbles are around $We \geq 100$ (when critical we is around 10 cause unstable and fragment into multiple small bubbles) and hard to maintain their shape and prone to deform in turbulent flow. However, we focused the possibilities on drag reduction and undiscovered phenomenon of large bubble. So, our research target aims to these large bubbles while other numerical studies are targeted relatively small bubble which has below $We = 1$ from (1-2).

In this study, we established numerical procedure how to inject the large bubble on turbulent channel flow without breakup. After then, we investigated the characteristics of large bubble from bubble shape to flow field.
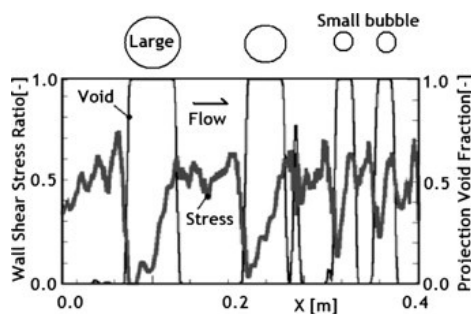

Fig. 1 Wall shear stress ratio as the size of bubbles

2. Characteristics of large bubble

The characteristics of large bubble are represented in Fig. 2 and can be divided into 2 parts as the bubble shape and flow field from (3). At first, bubble shape can be described that front side is spherical and smooth shape while rear side become tail which is

small portion of the bubble. In addition, upper side of rear region shows capillary wave in the streamwise direction.

Another characteristic is that this large bubble didn't break up even if We is over 100, and this value over critical weber number 10. However, the shape-fixing effect is provided by gravity. And they can survive in turbulent flow. Last, its attitude tilts downward on front side and maintains. About flow fields, skin friction on liquid film vary as the location of large bubble. As liquid film becomes thinner, skin friction decreases, and capillary wave makes minor effect on this phenomenon and describe in (4). After passing large bubble, there is secondary flow detached from rear region of bubble. In this region, they connected with main flow and skin friction takes locally high. In this study, we'll examine these phenomena in three-dimension, which hard to visualize in experiment. In addition, other flow fields such as vorticity structure and vector contours were examined.
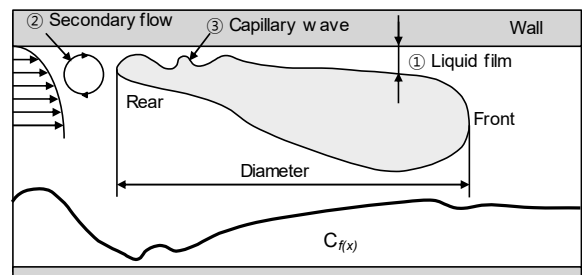

Fig. 2 Characteristics of large bubble (Murai et al., 2007)

3. Governing equations

In this study, two CFD solvers of OpenFOAM, one is *pimpleFoam* for one-phase flow and handy to generating turbulent channel flow, another is *interIsoFoam* for two-phase flow and main solver for turbulent channel flow with large bubble.

The flow is considered incompressible and the fluids are considered Newtonian. The governing equations in this study for continuity and momentum equation can be expressed as

$$\frac{\partial \rho}{\partial t} + \nabla \cdot (\rho u) = 0 \tag{1}$$

$$\frac{\partial \rho u}{\partial t} + \nabla \cdot (\rho u u) = -\nabla \cdot p + \nabla \cdot T + \rho f + f_\sigma \tag{2}$$

where, u is the fluid velocity, p is the pressure, T is stress tensor, f represent the body forces, and f_σ is the surface tension, respectively. In this study, the body force presents gravity and pressure gradient for cyclic conditions. For the VOF method, transport equation of the volume fraction α is like following.

$$\frac{\partial \alpha}{\partial t} + \nabla \cdot (\alpha u) = 0 \tag{3}$$

On the interface sharping method, *interIsoFoam* implements *isoAdvector* scheme. The *isoAdvector* method uses the concept of iso-surfaces to calculate more accurate face fluxes for the cells containing the interface and can be expressed as

$$a_i(t) = \frac{1}{V_i} \int_{\Omega_i} H(x,t)dV, \quad H(x,t) \equiv \frac{\rho(x,t) - \rho_B}{\rho_A - \rho_B} \tag{4}$$

$$a_i(t + \Delta t) = a_i(t) - \frac{1}{V_i} \sum_{j \in B_i} S_{ij} \Delta V_j(t, \Delta t) \tag{5}$$

Where, $a_i(t)$ is the value for the phase fraction in cell i at time t, $H(x,t)$ is indicator field function, V_i is the volume of cell i and Ω_i represents each cell. B_i is the list of all faces $\mathcal{F}_j$ belonging to cell i, S_{ij} is used to orient the flux to going out from the cell, and $\Delta V_j(t, \Delta t)$ describes the total volume of fluid transported across face j during one time-step.

4. NUMERICAL METHOD

4.1. Numerical setup

Before starting the simulation, it was checked previous experimental study to benchmark on the numerical simulation. So, the experimental condition, which is conducted by (5), was reviewed like following. In the case of channel's main properties, channel height and mean velocity are 10mm and 1m/s, respectively.

Other properties are like below Table. 1. To compare with numerical results, detail bubble properties were calculated like Table 2 based on Fig. 3. When calculating bubble volume, these bubbles needed to estimate to ellipsoid. In the case of domain size, it can be smaller than experiment thanks to cyclic condition, and number of mesh is 6.3million. The boundary conditions are shown in Fig. 4. and Table. 3 represents boundary conditions applied in each stage.

**Table 1.** Experimental condition (Oishi et al., 2014)

	Experiment	Present CFD
Channel size(mm)	10 x 100 x 6000	10 x 75 x 200
Liquid condition	Water (17°C)	
Density (kg/m^3)	998.7	
Kinematic viscosity (m^2/s)	1.08 x 10^{-6}	
Mean velocity (m/s)	1.0	
Froude number (-)	3.19	
Reynolds number (-)	9260	
Friction Reynolds number (-)	260	
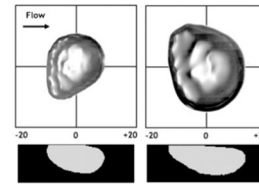
**Fig. 3** Bubble shape / Left: bubble 2, Right: bubble 3

Table 2. Properties of bubble

Diameter	Bubble 2	Bubble 3
Streamwise (mm)	10.14	12.97
Spanwise (mm)	11.559	14.75
Vertical (mm)	5.75	5.6
Volume (mm^3)	352.88	560.94
We	105	175
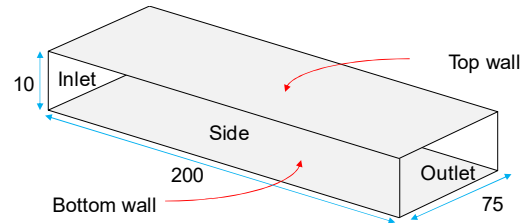
Fig. 4 Boundary conditions and domain size

Table 3. Boundary condition in each stage

	Stage 1		Stage 2		Stage 3
Solver	PimpleFoam	→	InterIsoFoam		
Inlet	Cyclic (Inlet ↔ Outlet)	→	Velocity Inlet	→	Cyclic (Inlet ↔ Outlet)
Outlet	Cyclic (Outlet ↔ Inlet)	→	Pressure Outlet	→	Cyclic (Outlet ↔ Inlet)
Side	Cyclic (Left ↔ Right)				
Bottom	Wall	→	Contact angle (1°)		
Top	Wall	→	Codestream (Inject)	→	Contact angle (1°)
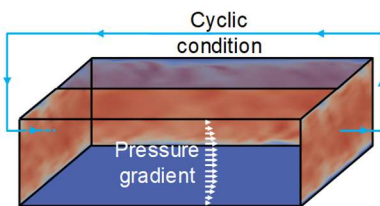
(a) Stage 1: Driver process for Turbulent flow
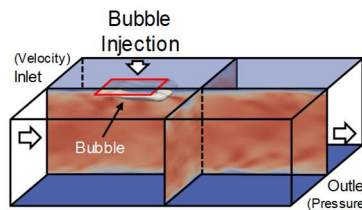
(b) Stage 2: Injection of bubble in channel
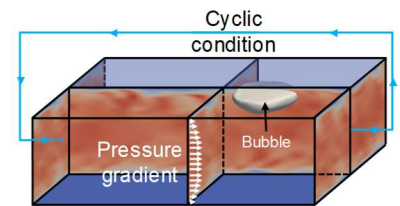
(c) Stage 3: Calculation until steady state

Fig. 5 Process of generating turbulent channel

4.2. Simulation procedure

As you can see in Fig. 5, the procedure of total simulation was divided into several stages. The reason is that current simulation is based on cyclic condition, so, injection condition like stage 2 cause error to the simulation and these cyclic conditions need to change.

To investigate bubble dynamics on the turbulent channel flow, we need to prepare fully developed boundary layers on the channel (Stage 1). In addition, we compared present results with experiment for the validation.

Fig. 6 represents the mean velocity profile and reynolds shear stress normalized by the friction velocity. As you can see, mean velocity resolved well until $y^+ < 20$ while there is overestimation from $y^+ = 20$. In the case of reynolds shear stress profiles, the circle is the experimental results. Both turbulent statistic profiles show good agreement. On the other hand, some difference shows from peak point from u_{rms} and underestimation in v_{rms}. It is considered that mesh is not refined as much as catching proper fluctuation, but overall trends follow experimental results reasonably. Thus, we conclude from these results that the present results are sufficiently reliable for evaluating the change due to inject a bubble in turbulent channel flow.

After generating turbulent channel flow with fully developed boundary layer, we investigated the way how to inject the bubble because large bubble is hard to inject due to high deformability. So, we've implemented *Codestream* for temporal inlet condition in the top wall, and we expected to acquire similar injected condition with experiment. In addition, Inlet and outlet condition switched to velocity inlet and pressure outlet from cyclic condition for avoiding continuity error. Eventually, the bubble injected and maintained its shape successfully, and the detail results are shown in Table. 4.
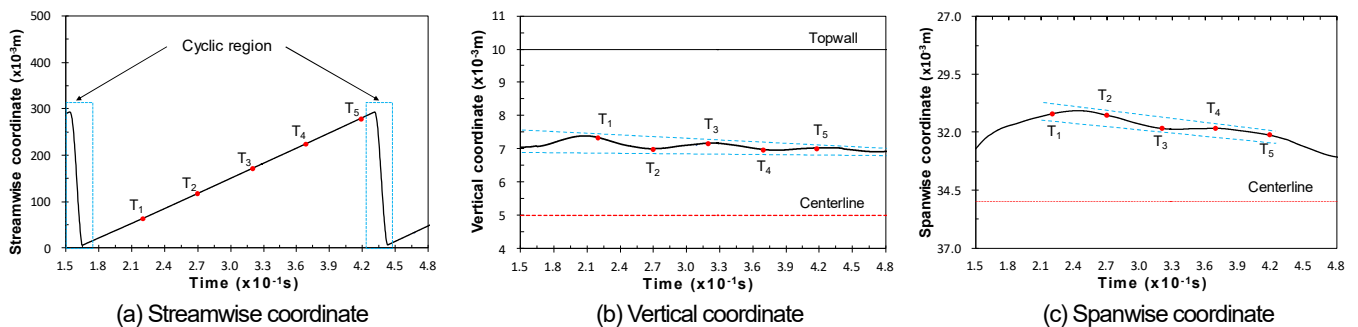
Table 4. Comparison of properties of injected bubbles

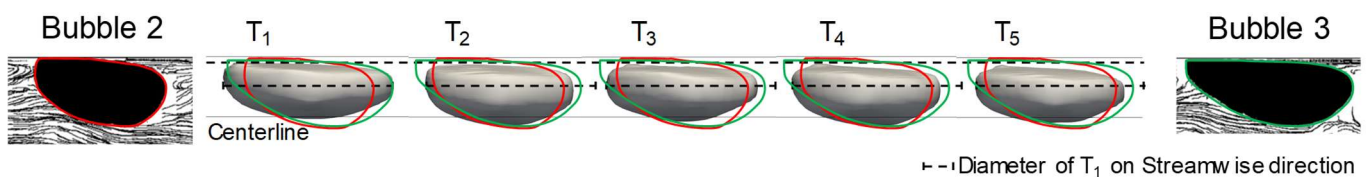| Diameter	Bubble 2	Bubble 3	Present CFD
Streamwise (mm)	10.14	12.97	12.4
Spanwise (mm)	11.559	14.75	13.5
Vertical (mm)	5.75	5.6	5.2
Volume (mm³)	352.88	560.94	460.36

The injected bubble needs to be detached from the wall for traveling around the channel, and fully developed boundary layer also needs to be sustained. So, the boundary conditions need to change cyclic conditions again. Also, the wall where applied *Codestream* has been switched to contact angle (1°C) condition for detaching from the wall. Therefore, the bubble successfully floats in the turbulent channel. Fig. 7 represents trajectories of the bubble in time domain. Among them, we selected specific points from $T_1 \sim T_5$, and they are visualized on the evolution of bubble shape in Figs. 8~9. Consequently, it shows good agreement with the experiment. First, it tilted downward and maintained its shape, but the liquid film looks like overestimated.

(a) Mean velocity   (b) Turbulent ratio   (c) Reynolds shear stress
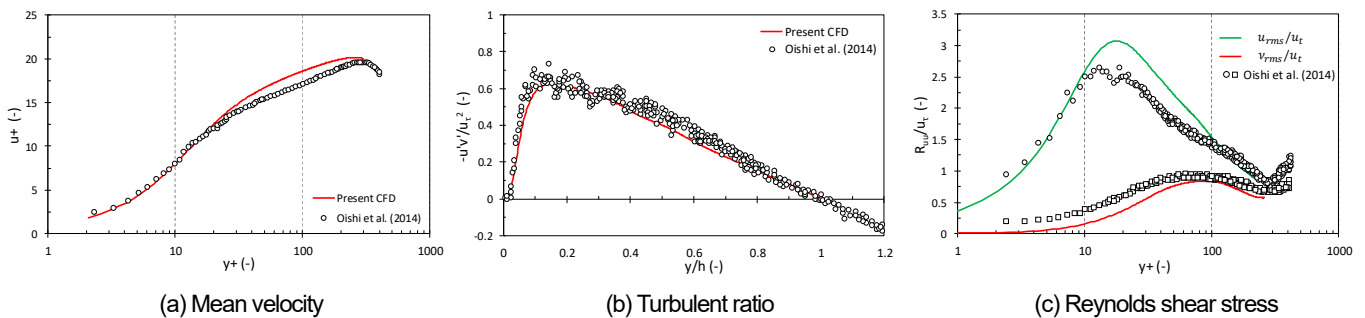
Fig. 6 Comparison on properties of turbulent channel flow

(a) Streamwise coordinate   (b) Vertical coordinate   (c) Spanwise coordinate

Fig. 7 Trajectories of the bubble

Fig. 8 Evolution of the bubble shape / side view
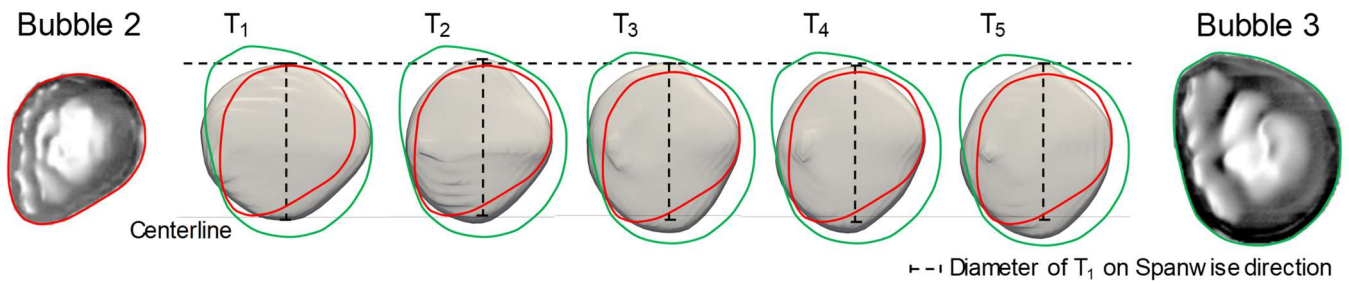
Copyright © 2019 by JSFM3

Fig. 9 Evolution of the bubble shape / top view

In addition, it was hard to observe flat shape in rear region of bubble. So, we considered that its shape originated from capillary wave while numerical results didn't catch. So, it is considered that skin friction also be overestimated than experiment. In the case of deformation and trajectories, we confirmed the bubble looks like bouncing on the top wall and become stable from Fig. 7-(b), and this oscillation caused expanding in vertical direction when shrinking in streamwise direction while the distance from the top wall is constant.

4. Numerical results and discussion

4.1. Iso-surfaces of the vorticity component

To see flow field around the bubble, we visualized iso-surface of vorticity component in streamwise direction, and the vorticity value are ±330, and it was shown in Fig. 10~11. From the top view, counter-rotating vorticity structure is not only observed from left and light side but also top and bottom side. These counter-rotating vortices between up and downside induced wake motion move outside and breakup itself after separating. From the side view, we can notice where these vortices originated. In the case of upside

vorticity, the vorticity originated and traveled on the top wall where is upside of the bubble. In addition, it is very thin and hard to catch from side view. On the other hand, the bottom vorticity is generated from the entire top of bubble surface and separated from the rear of bubble. Also, it attached to the top wall. Thus, two counter-rotating vortices attached to the top surface, and it consider one of the reasons that breakup vortices after separating.

4.2. Vector contours with relative velocity

In the case of vector contours, we observed two sections view from the center of bubble in Fig. 12~13. The velocity vector is calculated from relative velocity, and it can be expressed as

$$u(x, y, z) = u_0(x, y, z) - u_{mean}(x, y, z) \qquad (6)$$

Where, u_0 is velocity vector, u_{mean} is target velocity for pressure gradient and 1m/s in streamwise direction. First is the section on side view from bubble center.
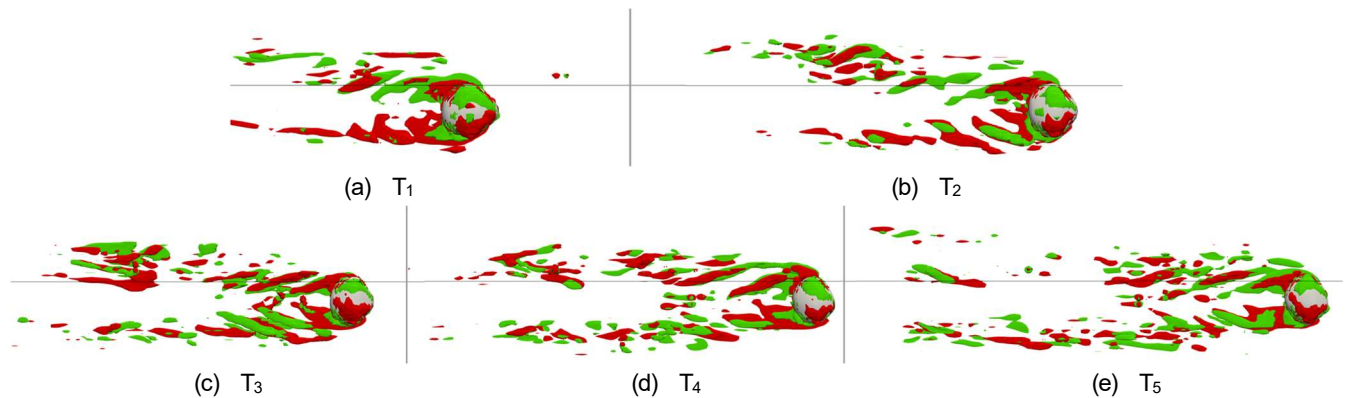

(a) T₁

(b) T₂

(c) T₃

(d) T₄

(e) T₅

Fig. 10 Top view of Snapshots on Iso-surface of vorticity x-component ($\omega_x = \pm330$)
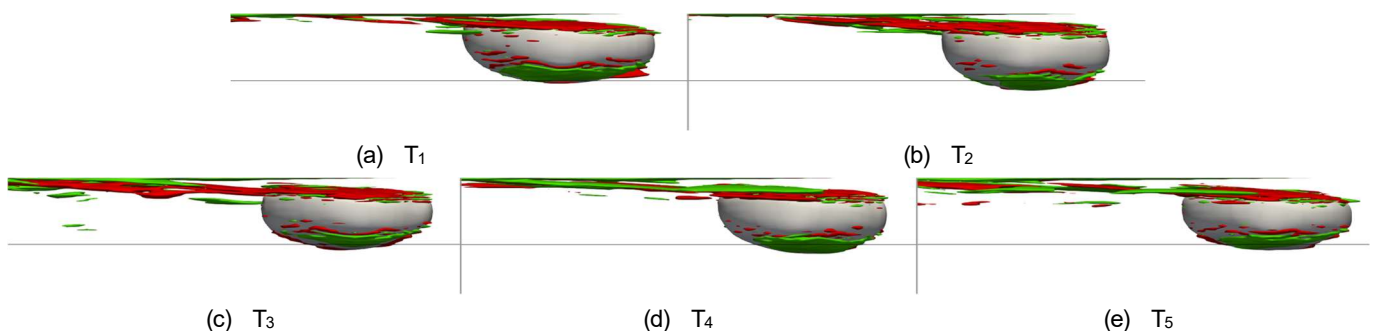

(a) T₁

(b) T₂

(c) T₃

(d) T₄

(e) T₅

Fig. 11 Side view of Snapshots on Iso-surface of vorticity x-component ($\omega_x = \pm330$)

shear stress on bubble surface. As a result, these fluctuations are not constant but considered that they coincide with the turbulent fluctuation of front side.
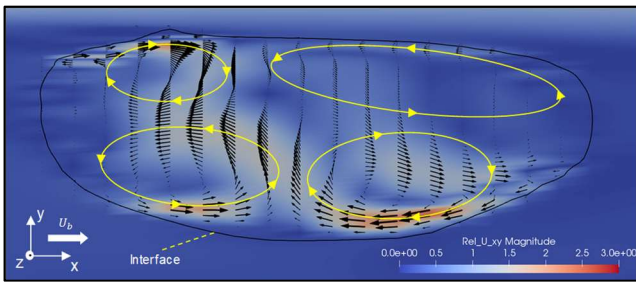

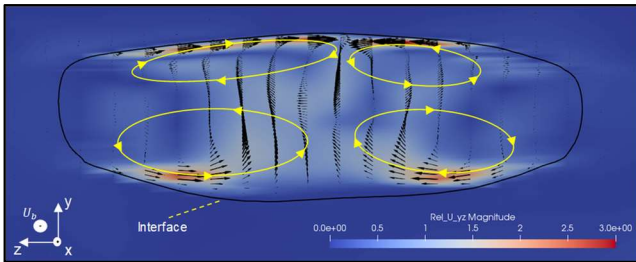Fig. 12 Vector contours with relative velocity / streamwise (x-y)

Fig. 13 Vector contours with relative velocity / Spanwise (y-z)

From there, we can see several vortexes inside of bubble. From the section of vertical and spanwise direction, we can clearly observe four vortexes inside of bubble. Based on the rotating direction, we can understand the reason why large bubble shape formed like figure. From streamwise section, the pair of upper side vortices rotate counter-direction, and this cause instantaneous velocity head downside to center of the bubble. This is also same on the pair of bottom side vortices which is instantaneous velocity head upper side. In the case of the pair vortices of front and rear side, instantaneous velocity head to outside. So, the bubble formed compression in vertical direction and wide in streamwise direction. This phenomenon occurred same from spanwise section.

In addition, we could estimate why vorticity of bottom surface of the bubble formed opposite direction to the upper side. On the other hand, the high velocity vector near the liquid film headed to the centerline of bubble.

4.3. Contours on bubble surface

As you can see from Fig. 14~16, we visualized vector and reynolds shear stress on bubble surface. In the case of vector contour from Fig. 14, the vectors originate from outside to the centerline and from front to rear on the top surface. This direction is corresponding with that of vector contour on spanwise section. On the other hand, the vectors headed to the bottom direction below the edge line of top surface. In the case of reynolds shear stress, we visualized profile on the centerline of bubble. In experiment, two case shows fluctuations of positive direction on rear (90°) but different fluctuations that bubble 3 has both directions of fluctuation while bubble 2 shows only positive direction on front (270°). As you can see from Fig.16, high shear stress to positive direction distributed on rear region like experiment and varied as the time. On bottom surface, numerical results didn't fluctuate in this region, and it is similar with bubble 2 while bubble 3 shows negative values. In addition, front region (200°~360°) also shows similar trends with bubble 2, but peak points located forward than experiment. These fluctuations varied as the time, and it is compared with reynolds
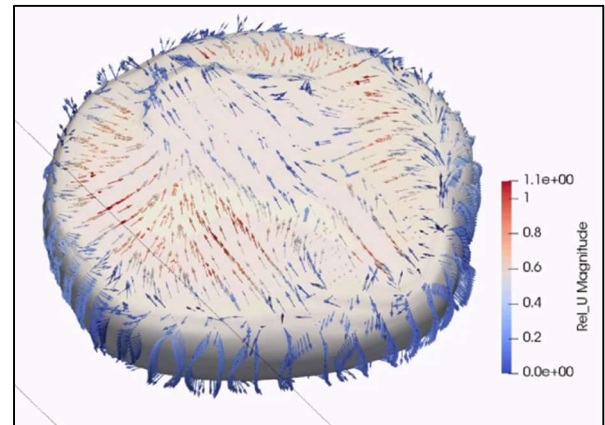

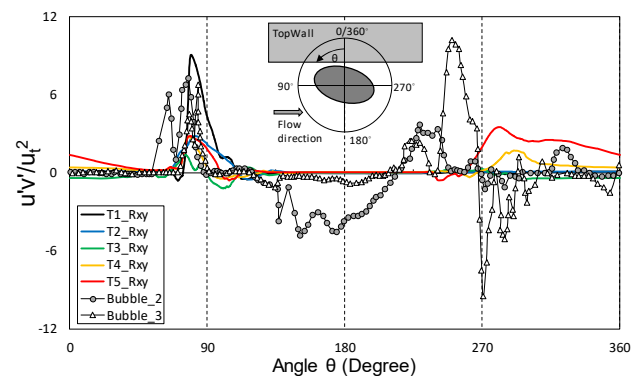Fig. 14 Vector contours on bubble surface / Time = T_3

Fig. 15 Reynolds shear stress on bubble surface as the angle

(a) T_1 (e) T_2 (e) T_3
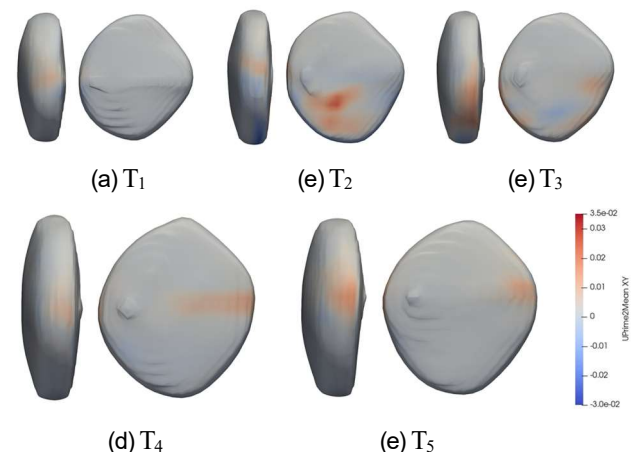
(d) T_4 (e) T_5

Fig. 16 Contour of reynolds shear stress on bubble surface

4.5. Wall shear stress

Last, the wall shear stress was observed. As you can see in Fig. 17 (Left), low shear stress observed in liquid film area while front side increased. In addition, there are locally high shear stress in secondary flow region. To compared as time sequence, the wall shear stress on bubble centerline extracted like Fig. 17 (Right). Figs. 18~19 represents the results wall shear stress that dotted line shows wall shear stress on liquid films. The global trends coincide

with explanation above. In detail, the wall shear stress slightly increased then gradually decreased as the location. Last, it suddenly reduced from certain point. And this point is corresponding with the region where is low velocity region after the peak point of interface in Fig. 12. In the case of secondary flow, the wall shear stress and vorticity magnitude were visualized. The vorticity magnitude is expressed as

$$\omega_{mag} = \sqrt{\omega_x{}^2 + \omega_y{}^2 + \omega_z{}^2} \tag{7}$$

Where ω_{mag} is vorticity magnitude, ω_x, ω_y, ω_z are vorticity x, y, z-component, respectively. And we can understand that vorticity structure (bright blue) which is attached on top surface coincides with peak regions of wall shear stress.

5.3. SUMMARY AND CONCLUSIONS

In this study, numerical simulations were conducted to figure out whether current CFD solver has capability for turbulent channel flow with large bubble. Also, the dynamic of a large bubble inside horizontal turbulent channel are investigated. And that can be achieved by separating 3 stages on numerical simulation.
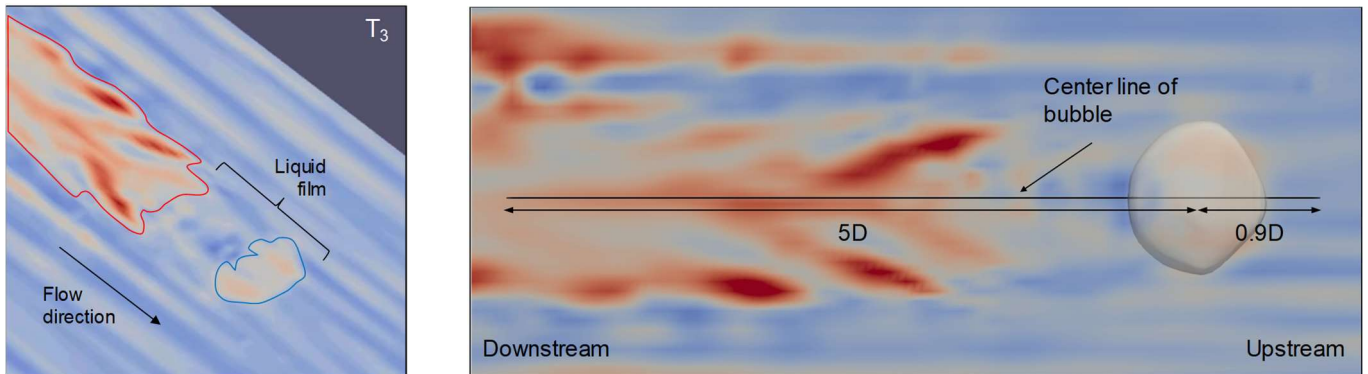

Fig. 17 Perspective view of Snapshot on Wall shear stress contours (Left), and Example of extracting wall shear stress profile (Right)
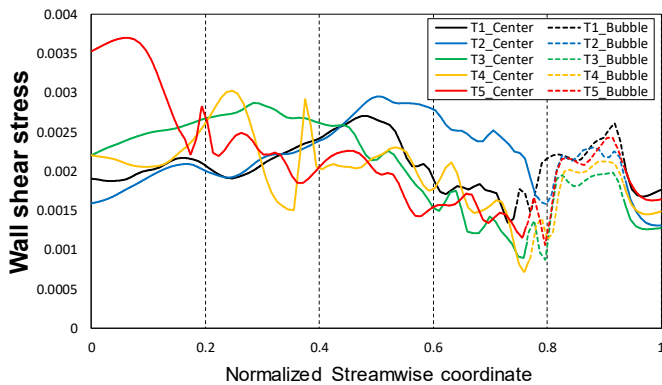

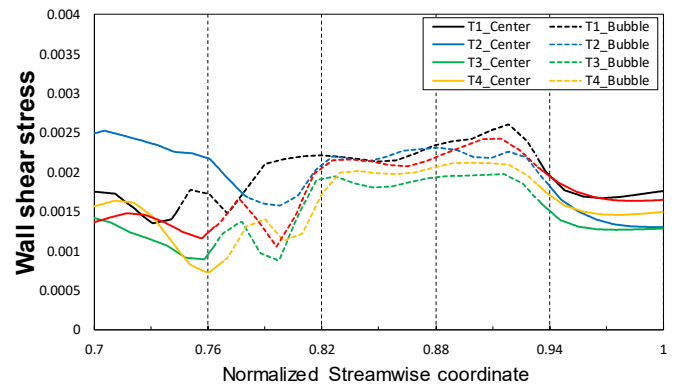Fig. 18 Wall shear stress profile as the time, dotted line: liquid film

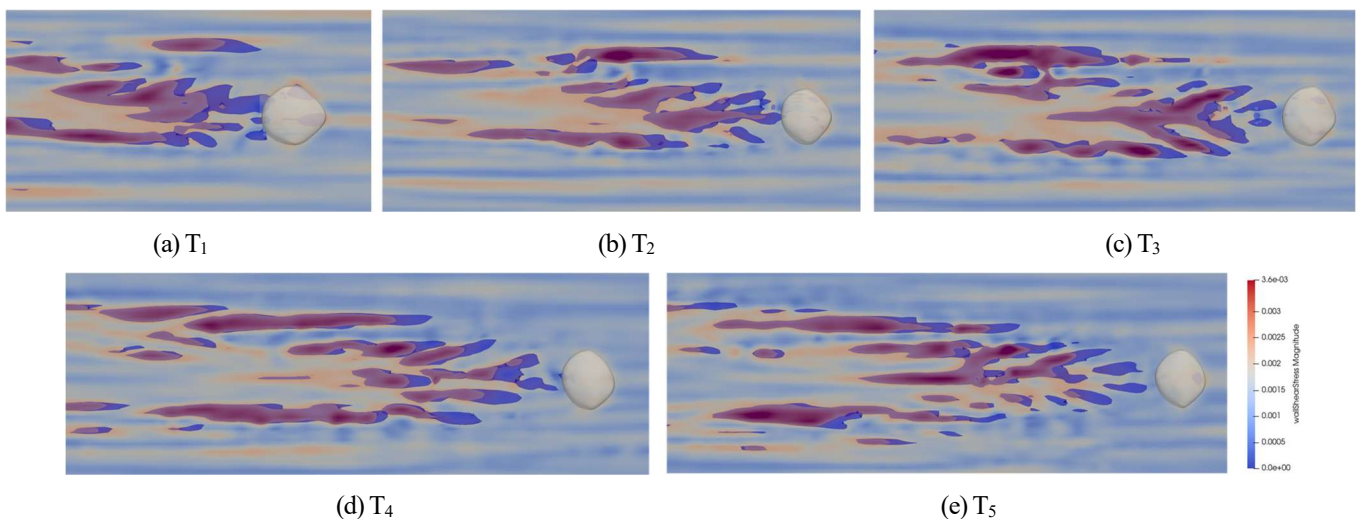Fig. 19 Wall shear stress near liquid films, dotted line: liquid film

(a) T_1　　　　　　(b) T_2　　　　　　(c) T_3

(d) T_4　　　　　　(e) T_5

Fig. 20 Contour of Wall shear stress and iso-surface of vorticity magnitude ($\boldsymbol{\omega_{mag}}$ = 500)

Still, it needed to optimize this procedure. The numerical results are compared with those of experiment to show the similarities and differences, and we could observe characteristics of large bubble such as liquid film, capillary wave and secondary flow. In future work, optimization and refinement of numerical condition were needed. In addition, effect of aligned single bubble will be investigated. To achieve it, it requires that each bubble needs to maintain constant distant between each bubble. This situation is hard to conduct in experimental, numerical simulation is easy to handle it thank to cyclic condition with single bubble.

Acknowledgments

Bibliography

(1) J. Lu, A. Fernandez, G. Tryggvason, the effect of bubbles on the wall drag in a turbulent channel flow, Physics of Fluids, Vol. 17, Issue 9 (2005), DOI: 10.1063/1.2033547

(2) Y. Yamamoto, T. Kunugi, Direct Numerical Simulation of Turbulent Channel Flow with Deformed Bubbles, Progress in Nuclear Science and Technology, Vol. 2 (2011): 543-549

(3) Y. Murai, H. Fukuda, Y. Oishi, Y. Kodama, F. Yamamoto, Skin friction reduction by large air bubbles in a horizontal channel flow, International Journal of Multiphase Flow, Vol. 33, Issue 2 (2007): 147-163, DOI: 10.1016/j.ijmultiphaseflow.2006.08.008

(4) P. Tisne, F. Aloui, L. Doubliezm Analysis of wall shear stress in wet foam flows using the electrochemical method, International Journal of Multiphase Flow, Vol 29, Issue 5 (2003): 841-854, DOI: 10.1016/S0301-9322(03)00038-7

(5) Y. Oishi, Y. Murai, Horizontal turbulent channel flow interacted by a single large bubble, Vol. 55 (2014): 128-139, DOI: 10.1016/j.expthermflusci.2014.02.022